# Application of Quantum Optimal Control to Shaken Lattice Interferometry

Jieqiu Shao, Liang-Ying Chih, Mantas Naris, Murray Holland, and Marco M. Nicotra

Abstract—This paper demonstrates how quantum optimal control can be used to perform shaken lattice interferometry. The first objective is to translate the five fundamental stages of interferometry (splitting, propagation, reflection, counter propagation and recombination) into quantum optimal control problems parametrized by the time horizon of each stage. The timing of each stage is then studied in relationship to its overall influence on the interferometer performance. This is done by comparing the population distributions obtained for a range of different accelerations and using Fisher information to estimate the sensitivity of the resulting accelerometer. These encouraging results highlight the effectiveness of quantum optimal control for the the design of next-generation atombased interferometers.

#### I. Introduction

Light-based interferometry has been a useful tool for metrology since Michelson and Morley's experiments [1]. Applications of light-based interferometry cover a wide range of measurements, from rotational motion [2] to even gravitational waves [3]. The basic principle behind interferometers is to superimpose two beams of light that generate different interference pattern based on the variation of a quantity to be measured. As shown in Figure 1a, this is achieved by submitting a single beam of light to the five fundamental interferometry stages: Splitting, propagation, reflection, counter propagation and recombination.

Atom-based interferometry, first demonstrated in [4], is a relatively recent technology that is widely acknowledged to have the potential of achieving a higher degree of accuracy than its light-based equivalent. Atom-based interferometers have already been used to measure dark energy [5], gravitational waves [6], and gravity gradients [7]. Although atom-based interferometers are expected to revolutionize strategic applications such as space navigation [8] and gravity monitoring [9], the overall technology is still under development.

The pioneering work featured in [10] showed that the accuracy of atom-based interferometers can be improved by trapping the atoms in an optical lattice and using the lattice to perform the five stages of interferometry. Although the general feasibility of this approach (known as "shaken lattice interferometry") has been demonstrated experimentally [11], additional research is required to identify the most promising shaking function for achieving the behavior illustrated in Figure 1b. Prior work has mostly focused on data driven approaches such as Nelder-Mead [12] and Q-learning [13]. However, recent results suggest that quantum optimal control

The authors are with the University of Colorado, Boulder. This research is supported by the US National Science Foundation through the award QII-TAQS 1936303.

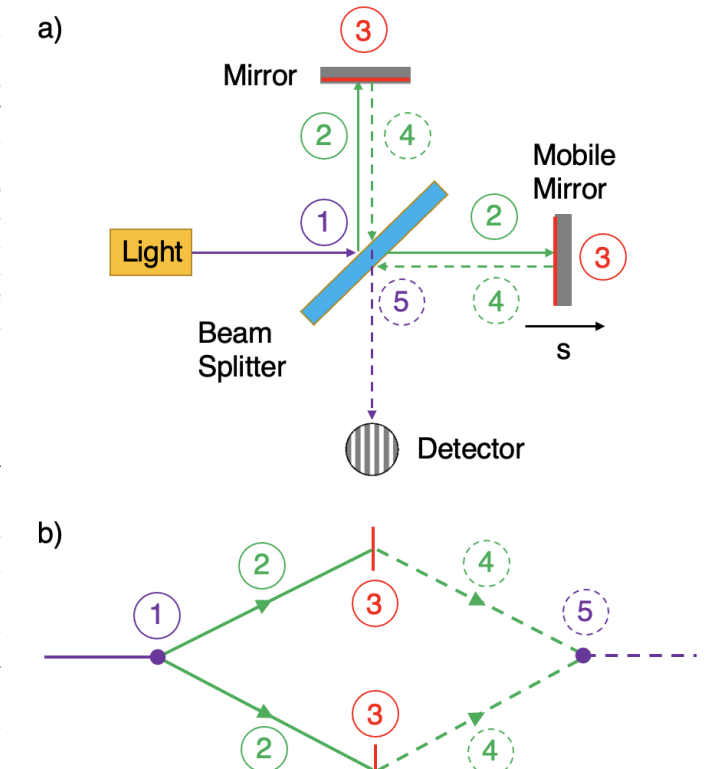


Fig. 1. a) The Michelson laser interferometer. First, the light is split into two beams that propagate until hit the mirror. After reflection, they counter propagate and are recombined. The interference pattern obtained at the recombination stage is then used to determine the position s of the mobile mirror. b) Ideal atom interferometer. The cloud of atoms is split into two clouds that propagate with opposite momentum. After reflection, they invert directions and finally recombine. The population distribution at the end of the recombination stage can theoretically be used to determine the acceleration acting on the system.

offers an attractive alternative for the robust and efficient manipulation of atoms trapped in an optical lattice [14].

The objective of this paper is to demonstrate that quantum optimal control can be used to succesfully perform shaken lattice interferometry. The timing requirements for each stage are characterized and numerical simulations are used to estimate the sensitivity of the resulting system when used as an accelerometer. The paper is organized as follows. Section II introduces the notations used in this paper. Section III presents the model for the shaken lattice interferometer. Section IV converts each of the five stages of interferometry into quantum optimal control problems. Section V discusses the timing of each stage and their effect on the interferometer.

Finally, Section VI shows how the shaken lattice interferometer can be used to measure accelerations.

#### II. NOTATION

For the purposes of this article, we use  $|\psi\rangle$  to denote a complex column vector and  $\langle\psi|$  to denote its complex-conjugate transpose. Given two unit vectors satisfying  $\langle\psi|\psi\rangle=1$  and  $\langle\nu|\nu\rangle=1$ , the two vectors are equal, i.e.,  $|\psi\rangle=|\nu\rangle$ , if and only if  $\langle\psi|\nu\rangle=1$ . The two vectors are instead equal up to a global phase  $\theta$ , i.e.,

$$\exists \theta \in [0, 2\pi) : |\psi\rangle = |\nu\rangle e^{i\theta}, \tag{1}$$

if and only if  $|\langle \psi | \nu \rangle| = 1$ . Given a matrix  $\Psi$ , we use  $||\Psi\rangle\rangle$  to denote the column-wise vector concatenation

$$\|\Psi\rangle\rangle = \left\| \begin{bmatrix} \downarrow & \downarrow & \dots & \downarrow \\ \psi_1 & \psi_2 & \dots & \psi_n \end{bmatrix} \right\| = \begin{bmatrix} \psi_1 \\ \psi_2 \\ \vdots \\ \psi_n \end{bmatrix}$$
 (2)

and  $\langle \Psi \|$  to denote the complex-conjugate transpose of  $\| \Psi \rangle$ . Moreover, we use  $0_n$ ,  $I_n$ , and  $J_n$  to denote the  $n \times n$  matrix of zeros, the identity matrix of size n, and the backward identity matrix of size n, respectively. Moreover, we use  $\otimes$  to denote the Kronecker product.

## III. MODELING

Consider a cloud of ultracold atoms trapped in an optical lattice. Let  $\mu$  denote the mass [kg] of the individual atoms and let  $k=2\pi/\lambda$  be the angular wavenumber of the laser beam, where  $\lambda$  is its wavelength [m]. As detailed in [15], the momentum distribution of this quantum system is governed by the Schrödinger equation

$$i |\dot{\psi}\rangle = H(u) |\psi\rangle,$$
 (4)

where  $|\psi(t)\rangle \in \mathbb{C}^n$  is the momentum distribution,  $u(t) \in \mathbb{R}$  is phase of the optical lattice,

$$H(u) = \omega_R (H_0 + H_1 \sin(u) + H_2 (1 - \cos(u))$$
 (5)

is the Hamiltonian, and  $H_0$ ,  $H_1$ ,  $H_2$  are given in (3). The model parameters are the recoil frequency  $\omega_R=\hbar k^2/2\mu$ , where  $\hbar\approx 1.055\cdot 10^{-34}{\rm J\,s}$  is the reduced Planck constant, the optical depth of the lattice  $\alpha=10$ , and the number of Bloch basis functions N=4 used to approximate the wavefunction, which ultimately determines the state vector length n=2N+1. To simplify the model, we assume hereafter  $\omega_R=1$  Hz, which is physically equivalent to measuring the system's timescale in units of  $\omega_R^{-1}$ .

## IV. CONTROL DESIGN

The objective of this section is to convert each of the five stages of interferometry into quantum optimal control problems to be solved using the approach detailed in [16].

## A. Propagation & Counter Propagation

The two propagation steps consist in letting the clouds of atoms move opposite to (or towards) each other. Rather than actively forcing the system, we wish to achieve a state of "free propagation" where the atoms have sufficient momentum to clear the peaks of the optical lattice on their own. To do so, consider the propagation period  $T_p > 0$  such that u(t) = 0,  $\forall t \in [0, T_p)$ . During this interval, the dynamic behaviour of (4)-(5) is

$$i |\dot{\psi}\rangle = H_0 |\psi\rangle$$
. (6)

Let  $\lambda_j$  and  $\nu_j$  be an eigenpair such that  $H_0 |\nu_j\rangle = \lambda_j |\nu_j\rangle$ . Given the initial condition  $|\psi(0)\rangle = |\nu_j\rangle \, e^{i\theta}$  with  $\theta \in [0,2\pi)$ , the analytical solution to the unforced system (6) is

$$|\psi(t)\rangle = |\nu_j\rangle e^{i(\theta - \lambda_j t)}, \quad \forall t \in [0, T_p),$$
 (7)

which satisfies  $\langle \psi(t)|\psi(0)\rangle=e^{-i\lambda_j t},\ \forall t\in[0,T_p).$  In other words, if  $|\psi(0)\rangle$  is an eigenstate of the free Hamiltonian  $H_0$ , the momentum distribution of the system will remain unchanged (up to a rotating global phase) as long as the control input satisfies u(t)=0.

To achieve free propagation, it is therefore sufficient to identify an eigenvector of  $H_0$  that features an equal and opposite momentum distribution. Due to the periodic nature of the optical lattice, this property is satisfied by every even-numbered eigenvector [17]. Figure 2 shows the momentum distribution of the fourth eigenvector  $|\nu_4\rangle$ , which was selected based on a trade-off between achieving a large splitting momentum, while also limiting the bandwidth of the shaking function required to achieve splitting.

## B. Splitting & Recombination

Having identified a suitable eigenstate for free propagation, the objective of the splitting step is to steer the quantum system from the ground state  $|\psi(0)\rangle = |\nu_1\rangle$ , which is the lowest-energy state where most atoms are trapped in the potential wells of the lattice, to the free propagation condition  $|\psi(T_s)\rangle = |\nu_4\rangle \, e^{i\theta}$ , where most ( $\approx 98\%$ ) of the atoms are propagating with a momentum of  $\pm 4\hbar k$ .

Since the global phase  $\theta \in [0,2\pi)$  is irrelevant, the control objective can be written in terms of minimizing the squared Hilbert-Schmidt distance  $\Delta(|\psi\rangle,|\nu_4\rangle) \coloneqq 1 - |\langle\psi|\nu_4\rangle|^2$ . This cost function, however, is non-convex with respect to  $|\psi\rangle$ . To obtain a convex formulation, we leverage the property  $\langle\psi|\psi\rangle=1$ , to rewrite the squared Hilbert-Schmidt distance

$$\Delta(|\psi\rangle, |\nu_4\rangle) = \langle \psi | P_4 | \psi \rangle, \tag{8}$$

where  $P_4 = I - |\nu_4\rangle\langle\nu_4|$  is a positive semidefinite matrix. The splitting function  $u_s(t), t \in [0, T_s)$ , can then be obtained by solving the quantum optimal control problem

min 
$$\frac{1}{2} \langle \psi(T_s) | P_4 | \psi(T_s) \rangle + \frac{1}{2} \int_0^{T_s} \rho u(t)^2 dt$$
 (9a)

s.t. 
$$i |\dot{\psi}\rangle = H(u) |\psi\rangle$$
,  $|\psi(0)\rangle = |\nu_0\rangle$ , (9b)

$$H_{0} = \begin{bmatrix} 4N^{2} & -\frac{\alpha}{4} \\ -\frac{\alpha}{4} & 4(N-1)^{2} & -\frac{\alpha}{4} \\ & \ddots & \ddots & \ddots \\ & & -\frac{\alpha}{4} & 4 & -\frac{\alpha}{4} \\ & & & -\frac{\alpha}{4} & 0 & -\frac{\alpha}{4} \\ & & & -\frac{\alpha}{4} & 4 & -\frac{\alpha}{4} \\ & & & & -\frac{\alpha}{4} & 4 & -\frac{\alpha}{4} \\ & & & & \ddots & \ddots & \ddots \\ & & & & -\frac{\alpha}{4} & 4(N-1)^{2} & -\frac{\alpha}{4} \\ & & & & -\frac{\alpha}{4} & 4N^{2} \end{bmatrix} \qquad H_{1} = \begin{bmatrix} 0 & i\frac{\alpha}{4} & 0 & i\frac{\alpha}{4} \\ -i\frac{\alpha}{4} & 0 & i\frac{\alpha}{4} & & \\ & & & -i\frac{\alpha}{4} & 0 & i\frac{\alpha}{4} \\ & & & & -i\frac{\alpha}{4} & 0 \end{bmatrix}$$

$$H_{2} = \begin{bmatrix} 0 & \frac{\alpha}{4} & & & \\ & & -i\frac{\alpha}{4} & 0 & i\frac{\alpha}{4} \\ & & & & -i\frac{\alpha}{4} & 0 \end{bmatrix}$$

$$H_{2} = \begin{bmatrix} 0 & \frac{\alpha}{4} & & & \\ & \frac{\alpha}{4} & 0 & \frac{\alpha}{4} & & \\ & & \frac{\alpha}{4} & 0 & \frac{\alpha}{4} \\ & & & \frac{\alpha}{4} & 0 \end{bmatrix}$$
(3)

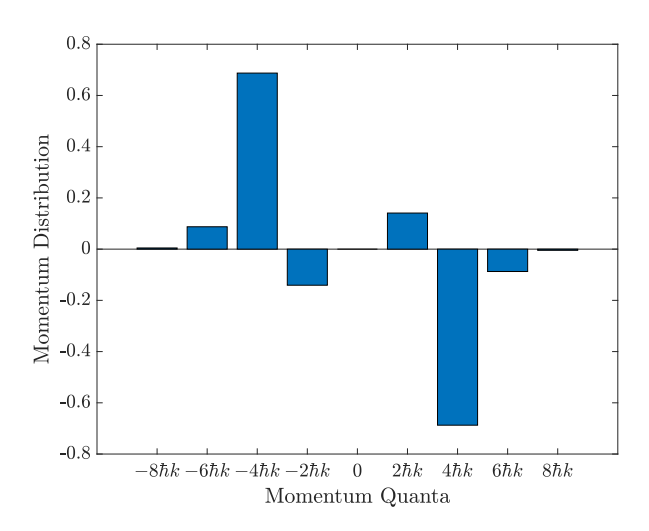


Fig. 2. Momentum distribution of the fourth eigenvector  $|\nu_4\rangle$  of the free Hamiltonian  $H_0$ . All atoms with a given momentum feature an equal counterpart with opposite momentum. Moreover, most ( $\approx 2~(0.7)^2 = 98\%$ ) of the atoms have a momentum of  $\pm 4\hbar k$ , which means that the system can be described by two large clouds are separating from each other with a relative momentum of  $8\hbar k$ .

where  $T_s>0$  is the splitting time (to be determined) and the scalar  $\rho=0.01$  penalizes the control effort while still being negligible with respect to the terminal cost.

As for the recombination step, its objective is to steer the system from the free counter-propagation eigenstate  $|\nu_4\rangle$  back to the ground state  $|\nu_1\rangle$ . Due to the reversable nature of quantum systems, the recombination function can be obtained by a simple time-reversal of the splitting function.

## C. Reflection

The objective of the reflection step is to invert the momentum of each atom cloud so that they all start propagating in the opposite direction. This can be achieved by performing a unitary transformation that maps the orthonormal basis  $||I_n\rangle\rangle$  onto its mirror opposite  $-||J_n\rangle\rangle$ . Unfortunately, the resulting optimization problem would feature a state vector of size  $n^2=(2N+1)^2$ , which is computationally intensive even for relatively small N.

To simplify the optimal control problem, we note that there

is no need to perform a full unitary transformation. Indeed, since the system is propagating in the fourth eigenstate, the reflection step can mostly be achieved by reflecting the eigenvector  $|\nu_4\rangle$  onto itself. With this in mind, consider

$$|\nu_{4}^{-}\rangle = \begin{bmatrix} I_{N} & & \\ & 0 & \\ & & 0_{N} \end{bmatrix} |\nu_{4}\rangle,$$

$$|\nu_{4}^{+}\rangle = \begin{bmatrix} 0_{N} & & \\ & 0 & \\ & & I_{N} \end{bmatrix} |\nu_{4}\rangle.$$
(10)

Since  $|\nu_4\rangle$  is a odd vector (i.e., it satisfies  $|\nu_4\rangle = -J_n |\nu_4\rangle$  as shown in Figure 2), we note that  $|\nu_4^+\rangle = -J_n |\nu_4^-\rangle$  and viceversa. Therefore, given the matrices

$$U_4^+ = [ |\nu_4^-\rangle | |\nu_4^+\rangle ], U_4^- = [ |\nu_4^+\rangle | |\nu_4^-\rangle ],$$

$$(11)$$

the reflection of the fourth eigenstate is achieved by mapping  $\|U_4^+\rangle\rangle$  onto its mirror opposite  $\|U_4^-\rangle\rangle=-J_n\|U_4^+\rangle\rangle$ . Given the matrix  $\Psi\in\mathbb{C}^{n\times 2}$ , the reflection step can then be written as the quantum optimal control problem

min 
$$\frac{1}{2} ||\Psi(T_r)\rangle\rangle - ||U_4^-\rangle\rangle|^2 + \frac{1}{2} \int_0^{T_r} \rho u(t)^2 dt$$
 (12a)

s.t. 
$$i\|\dot{\Psi}\rangle\rangle = [I_2 \otimes H(u)]\|\Psi\rangle\rangle$$
,  $\|\Psi(0)\rangle\rangle = \|U_4^+\rangle\rangle$ , (12b)

where  $T_r > 0$  is the reflection time (to be determined). Note that, unlike the splitting/recombination steps, the quantum optimal control problem (12) must account for the global phase of the system to achieve perfect reflection. This is done by penalizing the squared error of  $\|\Psi(T_r)\| - \|U_4^-\|$ . The solution to (12) is denoted as  $u_r(t)$ ,  $t \in [0, T_r)$ .

# V. INTERFEROMETER DESIGN

Having solved for the individual steps of the interferometer, we define the overall shaking function as

$$u(t) = \begin{cases} u_s(t), & t \in [0, T_1), \\ 0, & t \in [T_1, T_2), \\ u_r(t - T_2), & t \in [T_2, T_3), \\ 0, & t \in [T_3, T_4), \\ u_s(T_5 - t), & t \in [T_4, T_5), \\ 0, & t > T_5 \end{cases}$$
(13)

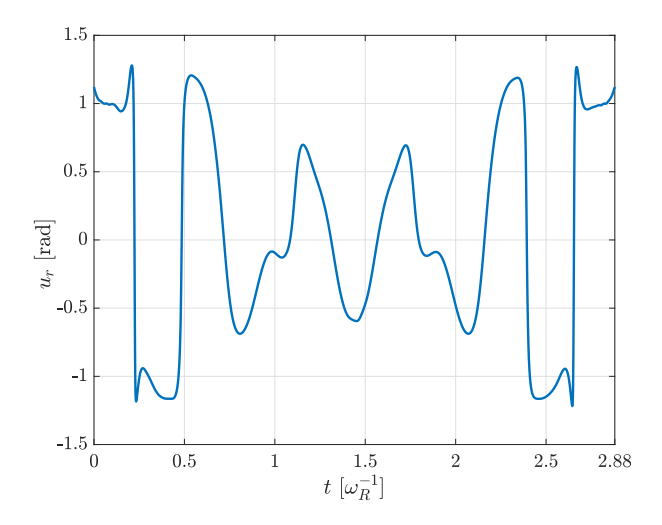


Fig. 3. Optimal shaking function obtained for the reflection step, given  $T_r=2.88\,\omega_R^{-1}$ . The function features a noticeable even symmetry, despite the fact that the quantum optimal control problem formulation (12) does not explicitly enforce any symmetry requirements.

where  $T_1 = T_s$ ,  $T_2 = T_1 + T_p$ ,  $T_3 = T_2 + T_r$ ,  $T_4 = T_3 + T_p$ , and  $T_5 = T_4 + T_s$ . This function is parameterized by the splitting time  $T_s$ , the propagation time  $T_p$ , and the reflection time  $T_r$ . Each of these parameters can significantly influence the sensitivity of the interferometer and will be addressed in the following subsections.

## A. Propagation Time

In analogy to classic interferometers, the sensitivity of the shaken lattice interferometer is proportional to the distance traveled by the atoms. Intuitively, the propagation time should therefore be "as large as possible", while being limited by the size of the instrument itself. Notably, the total distance traveled by a cloud of atoms of mass  $\mu$  propagating with a momentum of  $4\hbar k$  for a time of  $T_p$  would be

$$\Delta_p = \frac{4\hbar k}{\mu} T_p. \tag{14}$$

Given a realistic propagation distance of  $\Delta_p=1$  mm, the nominal propagation time would be  $T_p=922\,\omega_R^{-1}$ . For the purpose of this paper, however, we are going to limit ourselves to  $T_p=10\,\omega_R^{-1}$  due to the computational cost required to accurately solve the Schrödinger equation for the full range of accelerations detailed in Section VI. Note that, since u(t)=0 during the entirety of the propagation stage, the choice of  $T_p$  has no influence on the overall shape of the shaking function.

# B. Reflection Time

To pick a suitable reflection time  $T_r$ , it is important to note that the quality of reflection is very sensitive to the fundamental frequency of the shaking function  $u_r(t)$ . As detailed in [13], a suitable frequency for reflecting  $|\nu_4\rangle$  is the difference between the second and fourth eigenvalue, which equals  $12\omega_R$ . The reflection time can then be chosen as five

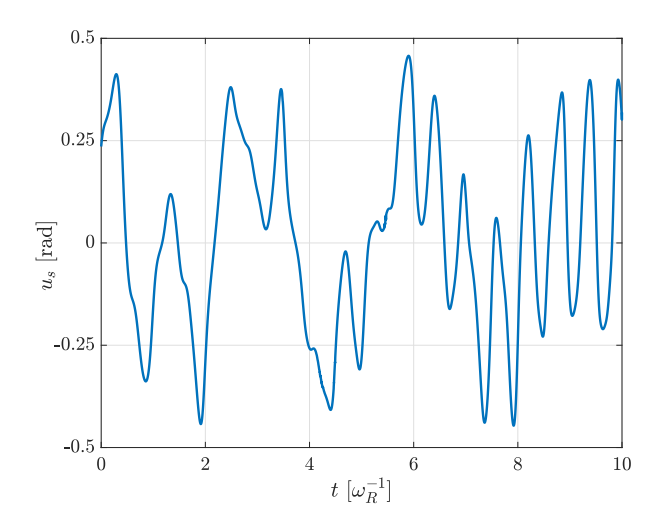


Fig. 4. Optimal splitting function obtained for  $T_s = 10 \,\omega_R^{-1}$ .

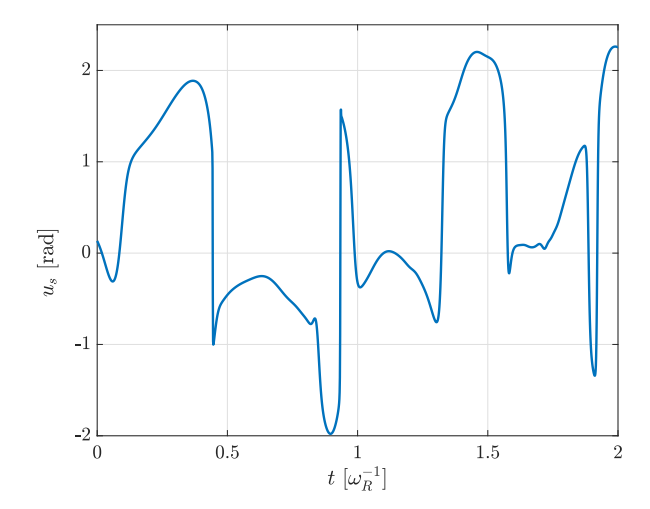


Fig. 5. Optimal splitting function obtained for  $T_s = 2 \omega_R^{-1}$ .

and a half cycles of the fundamental frequency, i.e.

$$T_r = 5.5 \cdot \frac{2\pi}{12\omega_R} \approx 2.88 \,\omega_R^{-1}.$$
 (15)

Interestingly enough, when this particular time horizon is used for the quantum optimal control problem (12), the resulting shaking function  $u_r(t)$  is symmetric (see Figure 3), despite the fact that symmetry is never explicitly enforced. This symmetry disappears when  $T_r$  is chosen arbitrarily.

## C. Splitting Time

The selection of an appropriate splitting time does not benefit from any particular guidelines. Intuitively, the splitting time should be "as short as possible" to mimic an instantaneous operation while still being sufficiently large to allow enough time for the atoms to react. Figures 4 and 5 illustrate the splitting function  $u_s(t)$  obtained for  $T_s=10\omega_R^{-1}$  and  $T_s=2\omega_R^{-1}$ , respectively. Their comparison suggests that longer splitting times require lower amplitudes

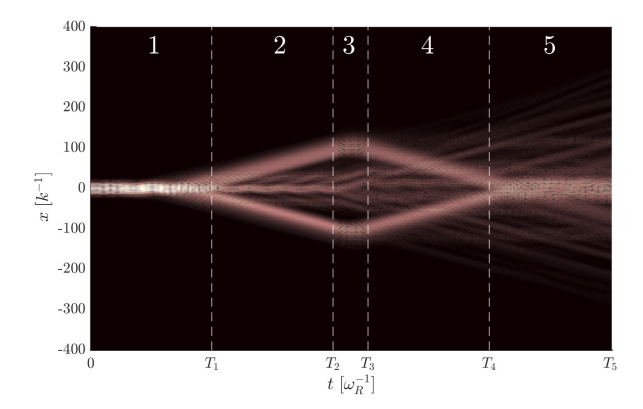


Fig. 6. Position distribution of the cloud of ultracold atoms during all five phases of the interferometer under zero acceleration, given a splitting time  $T_s=10~\omega_R^{-1}$ . Although many atoms split into two counter-propagating clouds, a significant number of atoms break off into unfocused beams that are not reflected and do not recombine at the end.

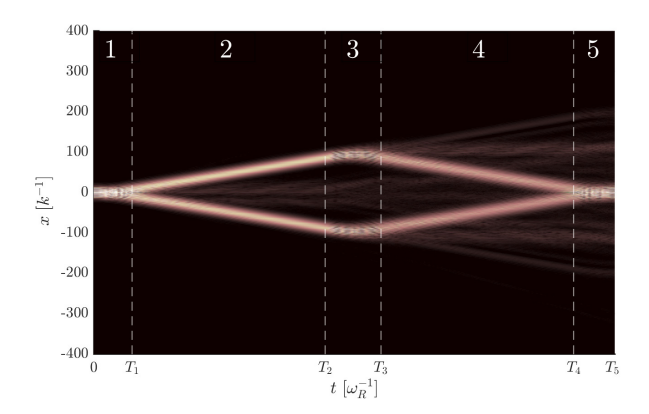


Fig. 7. Position distribution of the cloud of ultracold atoms during all five phases of the interferometer under zero acceleration, given a splitting time  $T_s=2\,\omega_R^{-1}$ . The atoms predominantly split into two clouds traveling with a momentum of  $\pm 4\hbar k$ , which are then reflected and recombined correctly. Although the figure still presents some undesirable tails, the majority of the atoms recombine in the same place where they started.

and smaller bandwidths, but provides little insight into which value is better suited for the interferometer.

To select a suitable splitting time, Figures 6 and 7 show the position distribution of the atom cloud when performing all five stages of the interferometer. These figures were obtained by convoluting the ground state  $|\nu_1\rangle$  with a narrow Gaussian function and computing the Fourier transform of the resulting momentum distribution. Comparison between these two figures shows that shorter splitting times provide better results (i.e. higher density of atoms propagating with a momentum of  $\pm 4\hbar k$ ) when considering realistic momentum distributions. Further reduction of the splitting time, i.e.  $T_s < 2\omega_R^{-1}$ , led to inadequate solutions of the quantum optimal control problem, thereby suggesting that the atoms need at least two units of recoil time to move from the ground state to the target eigenstate.

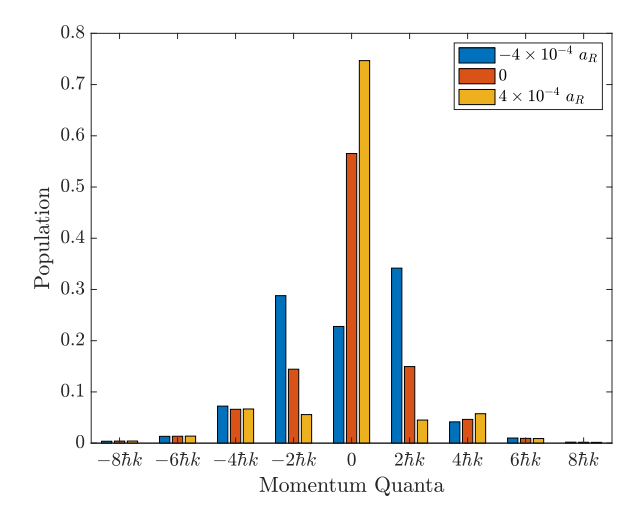


Fig. 8. Population distribution P(p|a) of three different acceleration values:  $a = -4 \times 10^{-4} a_R$ , a = 0, and  $a = 4 \times 10^{-4} a_R$ . Each acceleration features a very different population, making it possible to estimate the acceleration that gave rise to a specific population measurement.

## VI. ACCELEROMETER

Having obtained a suitable shaking function (13), the objective of this section is to perform a preliminary characterization of the expected performance for the shaken lattice interferometer. To this end, we first need to convert the dimensionless units used so far to the experimental units for real-world implementation. Notably, we consider rubidium atoms ( $\mu=1.44\times10^{-25}~{\rm kg}$ ), trapped in an optical lattice formed by counter-propagating laser beams with wavelength  $\lambda=852~{\rm nm}$ . We can then compute the recoil frequency

$$\omega_R = \frac{\hbar k^2}{2\mu} = \frac{\hbar (2\pi/\lambda)^2}{2\mu} = 1.99 \times 10^4 \text{ Hz}$$
 (16)

and the recoil acceleration

$$a_R = \omega_R \frac{\hbar k}{\mu} = 107 \text{ m/s}^2 \approx 10 \text{ g},$$
 (17)

where g is the gravitational acceleration.

The next step is to determine the behavior of the interferometer when subject to different accelerations. To this end, we simulate the response of the interferometer for a range of acceleration varying between  $\pm 6 \times 10^{-3} a_R \ (\pm 60 \ \mathrm{mg})$  with a resolution of  $\Delta a = 10^{-5} a_R \ (100 \ \mu g)$ . For each acceleration, we compute the momentum population distribution as

$$P(p|a) = |\psi(T_5)|_{N+1-p}^2, \qquad p \in [-N, N]$$
 (18)

where  $|\psi|_j$  is the absolute value of the j-th element of the complex vector  $|\psi\rangle$ . This quantity represents the probability that a momentum measurement will output the value  $2p\hbar k$ , given an acceleration a. For example, Figure 8 shows the population distributions P(p|a) obtained for three different accelerations  $a=-4\times 10^{-4}a_R$ , a=0, and  $a=4\times 10^{-4}a_R$ . Since the population distribution is unique for each acceleration, it can be used to solve the inverse problem of estimating the acceleration from a given population measurement.

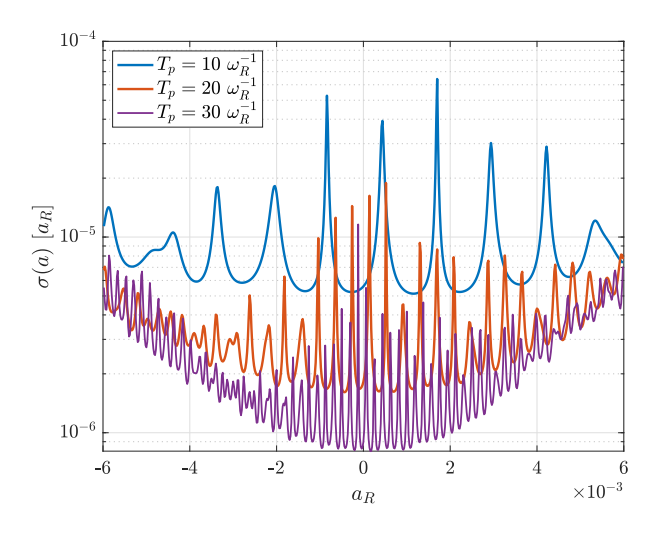


Fig. 9. Expected standard deviation of the measurement error obtained with the proposed interferometer, given  $M=10^4$  trapped ultracold atoms for different propagation times  $T_p$ . As  $T_p$  increases, the accuracy of the instrument also increases.

To characterize the sensitivity of the instrument (i.e., how well it is possible to recover the true acceleration value from a given population), we compute the Fisher information

$$I(a) = \sum_{p=-N}^{N} \frac{1}{P(p|a)} \left[ \frac{\partial P(p|a)}{\partial a} \right]^{2}, \tag{19}$$

which provides an approximate estimate for the accuracy of the accelerometer. Notably, the variance of the acceleration error satisfies

$$\sigma^2(a) \ge \frac{1}{I(a)M},\tag{20}$$

where  $M=10^4$  is the number of atoms trapped in the optical lattice. Figure 9 depicts the standard deviation of the acceleration error obtained for fairly small propagation times  $T_p$ . Even under these conditions, we note that the standard deviation is already quite reasonable, as it is represents a 0.1% error on the acceleration measurement. These results suggest that, for more a realistic propagation time  $T_p \approx 1000\,\omega_R^{-1}$ , the accuracy of the accelerometer could be as low as  $0.1\,\mu g$ . Proving this, however, would either require simulations with numerical accuracy that goes beyond the scope of this paper or experimental calibration.

# VII. CONCLUSION

This paper demonstrates that quantum optimal control can be used to successfully design a shaken lattice interferometer. After converting the five fundamental steps of interferometry into quantum optimal control problems, we find that the time horizons for each step play important roles in regard to the performance of interferometry: reflection is very sensitive to the control horizon and should be chosen based on the eigenvalues of the Hamiltonian, splitting should be as fast as possible to ensure a proper behavior for non-ideal momentum distributions, and propagation should be as long as possible to increase sensitivity. Numerical simulations showcase the

potential of the interferometer by using the Fisher information to quantify the expected standard deviation when the population distribution is used to estimate the acceleration acting on the system. These encouraging results represent a first step in the development of a new paradigm for atombased interferometry. Future work will focus on validating these control laws on experimental hardware, thereby verifying that each interferometer stage is performed correctly, and then calibrating the accelerometer to quantify its accuracy.

#### VIII. ACKNOWLEDGEMENTS

The authors would like to thank Dana Z. Anderson, Catie K. LeDesma, and Kendall Mehling for their insight on the experimental setup and its physical dimensions.

#### REFERENCES

- [1] R. S. Shankland, "Michelson-morley experiment," *American Journal of Physics*, vol. 32, no. 1, pp. 16–35, 1964.
- [2] N. Beverini, A. Di Virgilio, J. Belfi, A. Ortolan, K. Schreiber, A. Gebauer, and T. Klügel, "High-accuracy ring laser gyroscopes: Earth rotation rate and relativistic effects," in *Journal of Physics: Conference Series*, vol. 723, no. 1. IOP Publishing, 2016, p. 012061.
- [3] B. P. Abbott, R. Abbott, T. Abbott, M. Abernathy, F. Acernese, K. Ackley, C. Adams, T. Adams, P. Addesso, R. Adhikari et al., "Observation of gravitational waves from a binary black hole merger," *Physical review letters*, vol. 116, no. 6, p. 061102, 2016.
- [4] D. W. Keith, C. R. Ekstrom, Q. A. Turchette, and D. E. Pritchard, "An interferometer for atoms," *Physical review letters*, vol. 66, no. 21, p. 2693, 1991
- [5] P. Hamilton, M. Jaffe, P. Haslinger, Q. Simmons, H. Müller, and J. Khoury, "Atom-interferometry constraints on dark energy," *Science*, vol. 349, no. 6250, pp. 849–851, 2015.
- [6] S. Dimopoulos, P. W. Graham, J. M. Hogan, M. A. Kasevich, and S. Rajendran, "Gravitational wave detection with atom interferometry," *Physics Letters B*, vol. 678, no. 1, pp. 37–40, 2009.
- [7] M. Snadden, J. McGuirk, P. Bouyer, K. Haritos, and M. Kasevich, "Measurement of the earth's gravity gradient with an atom interferometer-based gravity gradiometer," *Physical review letters*, vol. 81, no. 5, p. 971, 1998.
- [8] M. Walport and P. Knight, "The quantum age: Technological opportunities," Blackett Review. UK Gov. Office for Science, 2016.
- [9] X. Ma, J. Fang, and X. Ning, "An overview of the autonomous navigation for a gravity-assist interplanetary spacecraft," *Progress in Aerospace Sciences*, vol. 63, pp. 56–66, 2013.
- [10] S. Pötting, M. Cramer, and P. Meystre, "Momentum-state engineering and control in bose-einstein condensates," *Physical Review A*, vol. 64, no. 6, p. 063613, 2001.
- [11] C. Weidner and D. Z. Anderson, "Experimental demonstration of shaken-lattice interferometry," *Physical Review Letters*, vol. 120, no. 26, p. 263201, 2018.
- [12] C. Weidner, H. Yu, R. Kosloff, and D. Z. Anderson, "Atom interferometry using a shaken optical lattice," *Physical Review A*, vol. 95, no. 4, p. 043624, 2017.
- [13] L.-Y. Chih and M. Holland, "Reinforcement-learning-based matterwave interferometer in a shaken optical lattice," *Physical Review Research*, vol. 3, no. 3, p. 033279, 2021.
- [14] N. Dupont, G. Chatelain, L. Gabardos, M. Arnal, J. Billy, B. Peaude-cerf, D. Sugny, and D. Guéry-Odelin, "Quantum state control of a bose-einstein condensate in an optical lattice," *PRX Quantum*, vol. 2, no. 4, p. 040303, 2021.
- [15] M. M. Nicotra, J. Shao, J. Combes, A. C. Theurkauf, P. Axelrad, L.-Y. Chih, M. Holland, A. A. Zozulya, C. K. LeDesma, K. Mehling, and D. Z. Anderson, "Modeling and control of ultracold atoms trapped in an optical lattice: An example-driven tutorial on quantum control," *IEEE Control Systems Magazine*, vol. 43, no. 1, pp. 28–43, 2023.
- [16] J. Shao, J. Combes, J. Hauser, and M. M. Nicotra, "Projection-operator-based newton method for the trajectory optimization of closed quantum systems," *Physical Review A*, vol. 105, no. 3, p. 032605, 2022
- [17] C. Kittel, Introduction to Solid State Physics (Seventh Edition). John Wiley & Sons, 1996.